

## Article

# Effect of Electroless Cu Plating $\text{Ti}_3\text{AlC}_2$ Particles on Microstructure and Properties of $\text{Gd}_2\text{O}_3/\text{Cu}$ Composites

Haiyao Cao, Zaiji Zhan \*  and Xiangzhe Lv 

State Key Laboratory of Metastable Materials Science & Technology, Yanshan University, Qinhuangdao 066004, China; haiyaocao@ysu.edu.cn (H.C.); lvxiangzhe@hotmail.com (X.L.)

\* Correspondence: zjzhan@ysu.edu.cn

**Abstract:**  $\text{Ti}_3\text{AlC}_2$  presents a hexagonal layered crystal structure and bridges the gap between metallic and ceramic properties, and Gadolinia ( $\text{Gd}_2\text{O}_3$ ) has excellent thermodynamic stability, which make them potentially attractive as dispersive phases for Cu matrix composites. In this paper,  $\text{Cu}@\text{Ti}_3\text{AlC}_2\text{-Gd}_2\text{O}_3/\text{Cu}$  composites,  $\text{Ti}_3\text{AlC}_2\text{-Gd}_2\text{O}_3/\text{Cu}$  composites, and  $\text{Gd}_2\text{O}_3/\text{Cu}$  composites were prepared by electroless Cu plating, internal oxidation, and vacuum hot press sintering. The microstructure and the effect of the Cu plating on the properties of the  $\text{Cu}@\text{Ti}_3\text{AlC}_2\text{-Gd}_2\text{O}_3/\text{Cu}$  composites were discussed. The results showed that a Cu plating with a thickness of about  $0.67\ \mu\text{m}$  was successfully plated onto the surface of  $\text{Ti}_3\text{AlC}_2$  particles. The ex situ  $\text{Ti}_3\text{AlC}_2$  particles were distributed at the Cu grain boundary, while the in situ  $\text{Gd}_2\text{O}_3$  particles with a grain size of 20 nm were dispersed in the Cu grains. The electroless Cu plating onto the surface of the  $\text{Ti}_3\text{AlC}_2$  particles effectively reduces their surfactivity and improves the surface contacting state between the  $\text{Cu}@\text{Ti}_3\text{AlC}_2$  particles and the Cu matrix, and reduces electron scattering, so that the tensile strength reached 378.9 MPa, meanwhile, the electrical conductivity and elongation of the Cu matrix composites was maintained at 93.6 IACS% and 17.6%.

**Keywords:**  $\text{Cu}@\text{Ti}_3\text{AlC}_2\text{-Gd}_2\text{O}_3/\text{Cu}$  composites; electroless Cu plating; microstructure; electrical conductivity; mechanical properties



**Citation:** Cao, H.; Zhan, Z.; Lv, X. Effect of Electroless Cu Plating  $\text{Ti}_3\text{AlC}_2$  Particles on Microstructure and Properties of  $\text{Gd}_2\text{O}_3/\text{Cu}$  Composites. *Materials* **2022**, *15*, 1846. <https://doi.org/10.3390/ma15051846>

Academic Editors:  
Gianfranco Dell'Agli and Victor M. de la Prida Pidal

Received: 24 January 2022  
Accepted: 26 February 2022  
Published: 1 March 2022

**Publisher's Note:** MDPI stays neutral with regard to jurisdictional claims in published maps and institutional affiliations.



**Copyright:** © 2022 by the authors. Licensee MDPI, Basel, Switzerland. This article is an open access article distributed under the terms and conditions of the Creative Commons Attribution (CC BY) license (<https://creativecommons.org/licenses/by/4.0/>).

## 1. Introduction

Because of the ease of fabrication, high thermal and electrical conductivities, and excellent corrosion resistance, copper and its alloys are widely used in industrial machinery such as heat exchangers, the divertor components such as fusion reactors, electrical equipment (wiring and motors), and construction for plumbing [1–5]. Particle-reinforced Cu matrix composites strengthened by low-content reinforcement particles could have a high strength performance, but the scattering of electrons was inevitably increased due to the addition of heterogeneous particles in the Cu matrix, consequently reducing the electrical conductivity of the Cu matrix composites. Therefore, the preparation of a particle-reinforced Cu matrix composite with high tensile strength and high electrical conductivity is still a challenge at present.

The reinforced particles can be introduced by in situ synthesizing or ex situ addition into the Cu matrix composites [6–10]. The compressive strength of an in situ (1.0 wt%)  $\text{Al}_2\text{O}_3/\text{Cu}$  composite synthesized from powders obtained by electrical explosion of wire was increased nearly 1.6 times compared with pure copper, but its electrical conductivity decreased from 95%IACS to 72%IACS [6]. Another Cu matrix composite strengthened by 3.0 wt% ex situ  $\text{Al}_2\text{O}_3$  particles was fabricated using the hot-pressing method [7], the hardness of the composite increased nearly 1.5 times compared with pure copper, but its electrical conductivity was down to 77%IACS. The average size of the in situ and ex situ  $\text{Al}_2\text{O}_3$  particles was 30 nm and  $65\ \mu\text{m}$ , respectively. The composite strengthened by ex situ  $\text{Al}_2\text{O}_3$  particles had a weak interface between the  $\text{Al}_2\text{O}_3$  particle and the Cu matrix

because of their large misfit in lattice parameters, CTE, and elastic modulus. Cr plating on the surface of the  $\text{Al}_2\text{O}_3$  particles could improve surface contacting state between the reinforced particles and the Cu matrix [8], and the tensile strength of the  $\text{Cr@Al}_2\text{O}_3/\text{Cu}$  composites was improved comparing with the  $\text{Al}_2\text{O}_3/\text{Cu}$  composites. In summary, the advantages of the in situ synthesized method over the ex situ method included offering a smaller particle size with the improved surface contacting state between the reinforced phase and Cu matrix, so that a better reinforcement effect could be achieved.

Gadolinia ( $\text{Gd}_2\text{O}_3$ ) and many other rare earth oxides are more attractive as dispersive phases than  $\text{Al}_2\text{O}_3$  for Cu matrix composites due to their excellent thermodynamic stability [11–14]. Moreover, those rare earth elements show a low diffusivity and solubility in the metal matrix because of their larger atomic radii, consequently, could improve the microstructural stability of the metal matrix against coarsening [15–18]. The addition of in situ synthesized  $\text{Y}_2\text{O}_3$  in Cu matrix led to the increase in ultimate tensile strength by nearly three times after cold rolling [11]. Therefore, the Cu matrix composites strengthened by in situ  $\text{Gd}_2\text{O}_3$  nanoparticles were expected to have both high tensile strength and high electrical conductivity.

MAX phases present a hexagonal layered crystal structure and bridge the gap between metallic and ceramic properties [19–23]. Comparing with  $\text{Al}_2\text{O}_3$ ,  $\text{TiB}_2$ , and  $\text{ZrB}_2$ ,  $\text{Ti}_3\text{AlC}_2$  presents high elastic moduli, high electrical conductivity, and low density relatively [24–27], which make  $\text{Ti}_3\text{AlC}_2$  a potentially attractive dispersion phase for Cu matrix composites. For example, Cu composite with 60 vol% ex situ  $\text{Ti}_3\text{AlC}_2$  particles prepared by ball milling for 10 h followed by hot press exhibited a superior ultimate compressive strength ( $1242 \pm 24$  MPa) and low electrical resistance ( $0.32 \times 10^{-6} \Omega\cdot\text{m}$ ) [19]. However, due to the limitation of in situ synthesized raw materials, reaction conditions, and reaction time, the content of in situ synthesized reinforcement phase is low, strengthening efficiency of the in situ reinforcement phase was limited, so the combination method of in situ synthesized and ex situ added reinforcement phase provides a way to prepare the particle-reinforced Cu matrix composites towards high tensile strength and high electrical conductivity, which was one innovation point of this paper.

The other innovation point of this paper was to prepare a Cu matrix composite with improved strength and stable electrical conductivity, the approach was to introduce in situ  $\text{Gd}_2\text{O}_3$  (internal oxidation) and ex situ  $\text{Ti}_3\text{AlC}_2$  (directly added) particles into a Cu matrix, and a layer of Cu was coated onto the surface of the  $\text{Ti}_3\text{AlC}_2$  particles before adding them into the Cu matrix to reduce their surfactivity and improve the surface contacting state between the  $\text{Cu@Ti}_3\text{AlC}_2$  particles and the Cu matrix. At the same time, the microstructure evolution and the effect of the Cu plating on the properties of the  $\text{Cu@Ti}_3\text{AlC}_2\text{-Gd}_2\text{O}_3/\text{Cu}$  composites were also discussed.

## 2. Materials and Methods

### 2.1. Raw Materials and Preparation Procedure

The raw materials for preparing  $\text{Cu@Ti}_3\text{AlC}_2\text{-Gd}_2\text{O}_3/\text{Cu}$  composites include Cu-Gd alloy powder (Central South University, Changsha, China), cuprous oxide ( $\text{Cu}_2\text{O}$ ) powder, and  $\text{Ti}_3\text{AlC}_2$  powder (Beijing Forsman Technology Co., Ltd, Beijing, China), their purities are above 99.0%, and their sizes are about 10, 2, and 2  $\mu\text{m}$ . The Cu-Gd alloy powder was atomized by high purity Ar gas from the inductive melting of Cu-Gd alloy ingots, which was made from Cu and Gd powders. The element content of Gd in Cu-Gd alloy powder is about 0.84 at% (2.04 wt%), which was analyzed using an X-ray fluorescence spectrometer (ARL, Switzerland).

Figure 1 presents the preparation process diagram of the  $\text{Cu@Ti}_3\text{AlC}_2\text{-Gd}_2\text{O}_3/\text{Cu}$  composite, which mainly included (a) electroless Cu plating on the surface of the  $\text{Ti}_3\text{AlC}_2$  particles, (b) in situ synthesis of  $\text{Gd}_2\text{O}_3$  reinforced phase, (c) the ball milling and sintering of the  $\text{Cu@Ti}_3\text{AlC}_2$  and  $\text{Gd}_2\text{O}_3/\text{Cu}$  powders.

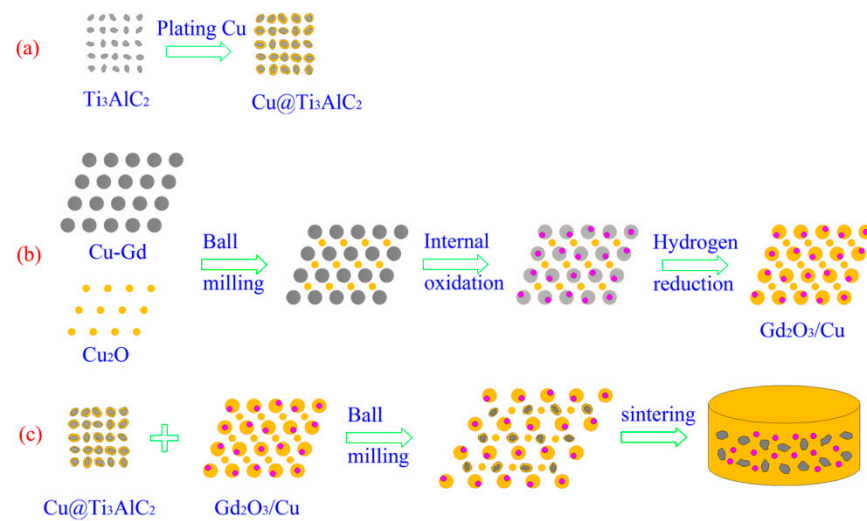
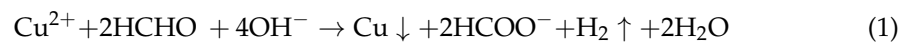


**Figure 1.** The preparation process diagram of the  $\text{Cu}@Ti_3AlC_2\text{-Gd}_2O_3/\text{Cu}$  composite: (a) electroless Cu plating on the surface of the  $\text{Ti}_3AlC_2$  particles, (b) in situ synthesis of  $\text{Gd}_2O_3$  reinforced phase, (c) the ball milling and sintering of the  $\text{Cu}@Ti_3AlC_2$  and  $\text{Gd}_2O_3/\text{Cu}$  powders.

### 2.1.1. Electroless Cu Plating on the Surface of the $\text{Ti}_3AlC_2$ Particles

Formaldehyde (HCHO) (Shanghai Aladdin Biochemical Technology Co., Ltd., Shanghai, China) was used as the reductant to coat Cu plating on the surface of  $\text{Ti}_3AlC_2$  particles in the bluestone solution ( $\text{CuSO}_4$ ), which could reduce the surfactivity of the  $\text{Ti}_3AlC_2$  particles, to enhance the surface contacting state between the  $\text{Ti}_3AlC_2$  particles and the Cu matrix. The reaction of electroless Cu plating on the surface of  $\text{Ti}_3AlC_2$  particles was followed by the Equation (1):



The electroless Cu plating process on the surface of  $\text{Ti}_3AlC_2$  particles mainly included the following steps: (a) pretreatment before electroless Cu plating, (b) electroless Cu plating process, and (c) treatment after electroless Cu plating.

(a) Pretreatment before electroless Cu plating: firstly, the  $\text{Ti}_3AlC_2$  particles were cleaned in acetone solution by ultrasonic bath for 10 min to remove the oil and other dirt attached on their surfaces. Then, the  $\text{Ti}_3AlC_2$  particles were stirred in a solution with a NaOH concentration of 30% and temperature of 363 K for 20 min using a constant temperature electromagnetic stirrer. Finally, the  $\text{Ti}_3AlC_2$  particles were cleaned with distilled water and dried in a vacuum oven.

(b) Electroless Cu plating process: the Cu electroless plating process was carried out in a constant temperature electromagnetic stirrer (INESA Scientific Instrument Co., Ltd., Shanghai, China) at a temperature of 333–338 K and a pH value of 12.0–12.5 with a stirring speed 60 r/min. Table 1 shows the composition and concentration of the bath solution used in electroless Cu plating on the surface of  $\text{Ti}_3AlC_2$  powder particles.

**Table 1.** The composition and concentration of bath solution.

Function	Main Salt	Reductant	pH Regulator	Stabilizer	Complex
Composition	$\text{CuSO}_4 \cdot 5\text{H}_2\text{O}$	HCHO (37%)	NaOH	2,2'-Bipyridyl	$\text{Na}_2\text{EDTA}$
Concentration	18 g/L	20 mL/L	8 g/L	0.05 g/L	30 g/L

The required concentration solution of  $\text{CuSO}_4 \cdot 5\text{H}_2\text{O}$  (Shanghai Aladdin Biochemical Technology Co., Ltd., Shanghai, China), 2,2'-bipyridine (Shanghai Aladdin Biochemical

Technology Co., Ltd., Shanghai, China), Na<sub>2</sub>EDTA (Shanghai Aladdin Biochemical Technology Co., Ltd., Shanghai, China), and NaOH (Shanghai Aladdin Biochemical Technology Co., Ltd., Shanghai, China) were prepared, respectively, before electroless Cu plating. Then, the prepared Na<sub>2</sub>EDTA solution, the NaOH solution, the 2,2'-bipyridine solution, and the Ti<sub>3</sub>AlC<sub>2</sub> powder particles were successively and slowly added into the CuSO<sub>4</sub> solution. During the whole electroless Cu plating process, the electromagnetic stirrer remained running to keep the mixed solution in a uniform condition. The HCHO solution was finally added into the mixture after the temperature reached to 333~338 K and the pH value between 12.0 and 12.5, then the Cu in the mixed solution began to deposit on Ti<sub>3</sub>AlC<sub>2</sub> particles.

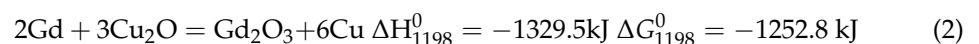
Due to the consumption of OH<sup>-</sup> ions and the generation of H<sub>2</sub> during the plating process, the pH value of the mixed solution would decrease, the NaOH solution should be continuously added into the mixed solution to keep the PH value between 12.0 and 12.5. As the electroless plating process went on, the Cu<sup>2+</sup> in the mixed solution was gradually reduced to Cu and deposited on the surface of Ti<sub>3</sub>AlC<sub>2</sub> powder particles, the color of the mixed solution gradually became lighter and lighter, and finally colorless and transparent, indicating that almost all the Cu<sup>2+</sup> in the mixed solution was consumed to Cu to deposit onto the surface of Ti<sub>3</sub>AlC<sub>2</sub> particles, and the electroless Cu plating process was over.

(c) Treatment after electroless Cu plating: after the reaction, the beaker with the mixed solution was removed from the electromagnetic mixer agitator (INESA Scientific Instrument Co., Ltd., Shanghai, China) and left for stratifying. The size and density of the Ti<sub>3</sub>AlC<sub>2</sub> particles were greatly increased as a layer of Cu grains was deposited onto the surface of Ti<sub>3</sub>AlC<sub>2</sub> particles after electroless plating. Therefore, the electroless Cu plating Ti<sub>3</sub>AlC<sub>2</sub> (Cu@Ti<sub>3</sub>AlC<sub>2</sub>) particles almost all sank at the bottom of the beaker after simple standing for a few minutes.

After pouring out the residual plating solution, distilled water and alcohol were repeatedly used to clean and wash the Cu@Ti<sub>3</sub>AlC<sub>2</sub> particles alternately three times, and the Cu@Ti<sub>3</sub>AlC<sub>2</sub> particles were then dried in a vacuum oven.

### 2.1.2. In Situ Synthesis of Gd<sub>2</sub>O<sub>3</sub> Reinforced Phase

The Gd<sub>2</sub>O<sub>3</sub> reinforced phase was in situ synthesized by internal oxidation method according to the following reaction Equation (2) [5]:



The Cu-Gd alloy powder and Cu<sub>2</sub>O powder were planetary ball milled for 4 h in an Ar atmosphere, the weight ratio of the ball-to-powder and milling speed were 4:1 and 180 rpm, respectively. Then, the mixed powders were oxidized in a vacuum furnace (0.3 Pa) at 1198 K for 1 h. Subsequently, the mixed powders were reduced by high purity hydrogen at 698 K for 2 h to remove excess oxygen, and finally the Gd<sub>2</sub>O<sub>3</sub>/Cu powder was obtained.

### 2.1.3. The Ball Milling and Sintering of the Cu@Ti<sub>3</sub>AlC<sub>2</sub> and Gd<sub>2</sub>O<sub>3</sub>/Cu Powders

A certain amount of Cu@Ti<sub>3</sub>AlC<sub>2</sub> powder and Gd<sub>2</sub>O<sub>3</sub>/Cu powder were planetary ball milled under the same milling condition in Section 2.1.2. Then, the mixed powders containing 1.5 wt% Ti<sub>3</sub>AlC<sub>2</sub> and 2.0 wt% Gd<sub>2</sub>O<sub>3</sub> were prepressed at 10 MPa, followed by sintering in a vacuum hot pressure sintering furnace (Shanghai Chenhua Science Technology Co., Ltd., Shanghai, China) ( $3.0 \times 10^{-2}$  Pa) at 1173 K for 30 min. The uniaxial pressure of 30 MPa and heating rate of 10 K/min were applied. Ti<sub>3</sub>AlC<sub>2</sub>-Gd<sub>2</sub>O<sub>3</sub>/Cu composites (1.5 wt% Ti<sub>3</sub>AlC<sub>2</sub> without electroless Cu plating and 2.0 wt% in situ Gd<sub>2</sub>O<sub>3</sub>) and Gd<sub>2</sub>O<sub>3</sub>/Cu composites (2.0 wt% in situ Gd<sub>2</sub>O<sub>3</sub>) were also prepared under the same conditions for comparison, a certain amount of spherical pure Cu powder (99.9% purity, ~10 μm in diameter) was added to maintain the same amount of reinforcement in the composites.

## 2.2. Test Methods

The morphologies and microstructures of the reinforced particles and the interfaces in the composites were conducted by scanning electron microscopy with an acceleration voltage of 25 kV (SEM, KYKY-EM3200, KYKY, Beijing, China) and transmission electron microscopy at 300 kV (TEM, Tecnai G2 F30, FEI, Hillsboro, OR, USA), which was equipped with an energy-dispersive X-ray spectrometric (EDS, Mahwah, NJ, USA) system. The ex situ  $\text{Ti}_3\text{AlC}_2$  powder, ex situ  $\text{Cu@Ti}_3\text{AlC}_2$  powder, the mixed powders of Cu-Gd alloy powder and  $\text{Cu}_2\text{O}$  powder before internal oxidation and after  $\text{H}_2$  reduction were evaluated by X-ray diffraction (XRD, D/MAX-2500/PC, Tokyo, Japan) method, respectively. The electrical conductivity of the samples was tested with a four probes method at ambient temperature, the tip distance of the four probes is 1 mm, and the size of the electrical conductivity sample is  $\varphi 30 \text{ mm} \times 4.5 \text{ mm}$ . Nine different areas in each sample were randomly selected for the electrical conductivity tests to minimize the error. A TH5000 universal testing machine (Jiangsu Tianhui Experimental Machinery Co., Ltd., Yangzhou, China) was used for tensile tests at ambient temperature according to GB/T 228.1-2010, the crosshead speed was 0.3 mm/min. The schematic diagram of the tensile specimens is shown in Figure 2, the gage length was 10 mm, and cross sections of  $2 \times 1.5 \text{ mm}$ , respectively. Three specimens were tested from each sintered billet for tensile and electrical conductivity tests to minimize the error. The average tensile strengths and elongation of the samples were calculated from the recorded tensile stress–strain curves.

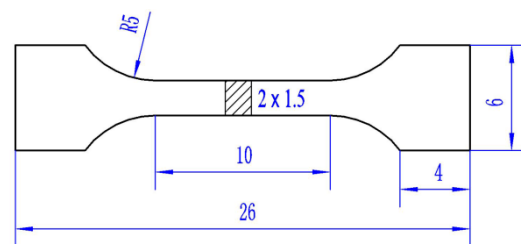
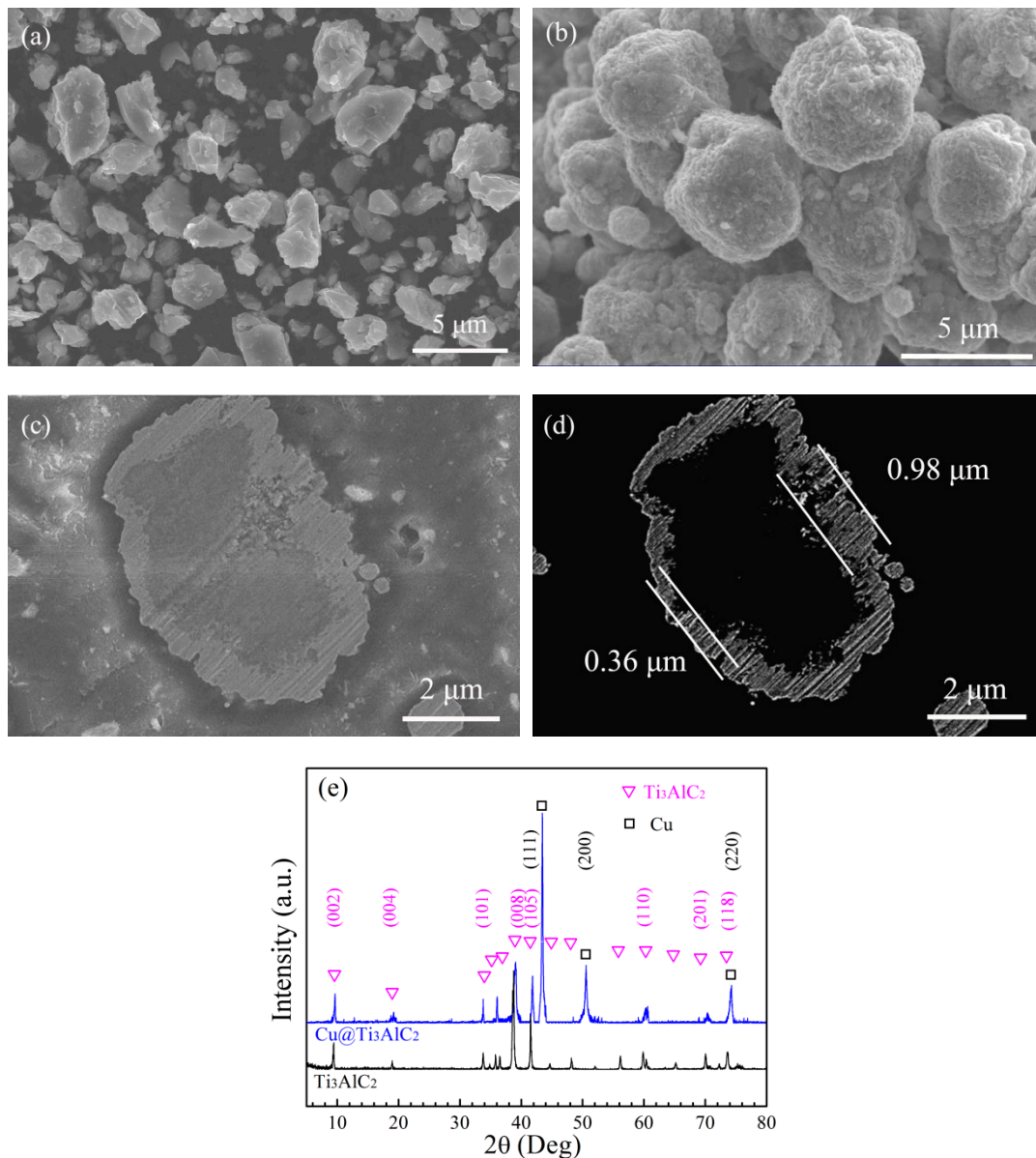


Figure 2. Schematic diagram of tensile specimen (unit: mm).

## 3. Results and Discussion

### 3.1. Electroless Cu Plating on the Surface of $\text{Ti}_3\text{AlC}_2$ Particles

The morphologies and XRD patterns of the  $\text{Ti}_3\text{AlC}_2$  powder and  $\text{Cu@Ti}_3\text{AlC}_2$  powder were conducted to analyze the quality of the Cu plating. Figure 3a shows the angular morphology of the  $\text{Ti}_3\text{AlC}_2$  particles with a size of about  $2 \mu\text{m}$ , the  $\text{Ti}_3\text{AlC}_2$  particles became smooth and ellipsoidal after electroless Cu plating (Figure 3b), and fine size Cu particles were uniformly distributed onto the  $\text{Ti}_3\text{AlC}_2$  particles' surfaces without micropores. From Figure 3c,d,  $\text{Ti}_3\text{AlC}_2$  particle was completely wrapped by the Cu plating without gaps or micropores, and the thickness of the Cu plating varied from  $0.36$  to  $0.98 \mu\text{m}$  and averaged  $0.67 \mu\text{m}$ . Figure 3e presents the XRD patterns of the  $\text{Ti}_3\text{AlC}_2$  powder and  $\text{Cu@Ti}_3\text{AlC}_2$  powder. Strong peaks of  $\text{Ti}_3\text{AlC}_2$  were seen in  $\text{Ti}_3\text{AlC}_2$  powder in Figure 3e; the characteristic peak of Cu was sharp and strong, while the characteristic peak of  $\text{Ti}_3\text{AlC}_2$  was weak in  $\text{Cu@Ti}_3\text{AlC}_2$  powder in Figure 3e ( $\text{Ti}_3\text{AlC}_2$ :PDF#52-0875, Cu: PDF#04-0836). The initial weight of  $\text{Ti}_3\text{AlC}_2$  powder was  $0.50 \text{ g}$ , which increased to  $4.11 \text{ g}$  ( $\text{Cu@Ti}_3\text{AlC}_2$ ) after electroless copper plating. The calculated average thickness of the Cu plating of  $0.66 \mu\text{m}$  was obtained according to the theoretical density of  $\text{Ti}_3\text{AlC}_2$  and pure Cu, the weight increment, and the size of  $\text{Ti}_3\text{AlC}_2$ ; the value was close to the average value in Figure 3d.



**Figure 3.** The  $\text{Ti}_3\text{AlC}_2$  powder particles before and after electroless Cu plating: (a,b) the morphology of  $\text{Ti}_3\text{AlC}_2$  powder and  $\text{Cu@Ti}_3\text{AlC}_2$  powder; (c,d) the profile of the  $\text{Cu@Ti}_3\text{AlC}_2$  powder; (e) the XRD patterns of  $\text{Ti}_3\text{AlC}_2$  powder and  $\text{Cu@Ti}_3\text{AlC}_2$  powder.

### 3.2. In Situ Synthesis of $\text{Gd}_2\text{O}_3$

Figure 4 shows the powder analysis of in situ synthesis of  $\text{Gd}_2\text{O}_3$ , and Figure 4a presents SEM images of Cu-Gd alloy powder mixed with  $\text{Cu}_2\text{O}$  powder before internal oxidation. The diffusing distance of O in the  $\text{Cu}_2\text{O}$  into the Cu-Gd alloy powder was reduced because the fine  $\text{Cu}_2\text{O}$  powder adhered to the surface of the larger Cu-Gd alloy powder after ball milling, which was beneficial to the reaction between the Gd in Cu-Gd alloy powder and O in  $\text{Cu}_2\text{O}$  powder during the internal oxidation process, and the synthesis of  $\text{Gd}_2\text{O}_3$  would be easier and more efficient. Figure 4b shows the SEM images of Cu-Gd alloy powder mixed with  $\text{Cu}_2\text{O}$  powder after  $\text{H}_2$  reduction, the  $\text{Cu}_2\text{O}$  powder adhering to the surface of Cu-Gd alloy powder gradually integrated after the mixed powder was oxidized at 1198 K for 1h and reduced by  $\text{H}_2$  at 698K for 2 h, meanwhile, the surface of the mixed powders became rougher. Figure 4c presents the XRD patterns of the mixed powders in Figure 4a,b, a weak characteristic peak of  $\text{Gd}_2\text{O}_3$  (222) could be seen in the XRD patterns of the mixed powders after internal oxidation and  $\text{H}_2$  reduction, indicating that

Gd<sub>2</sub>O<sub>3</sub> reinforced phase was in situ synthesized. At the same time, the characteristic peak of Cu<sub>2</sub>O disappeared, indicating that Cu<sub>2</sub>O was reacted to Cu during the H<sub>2</sub> reduction.

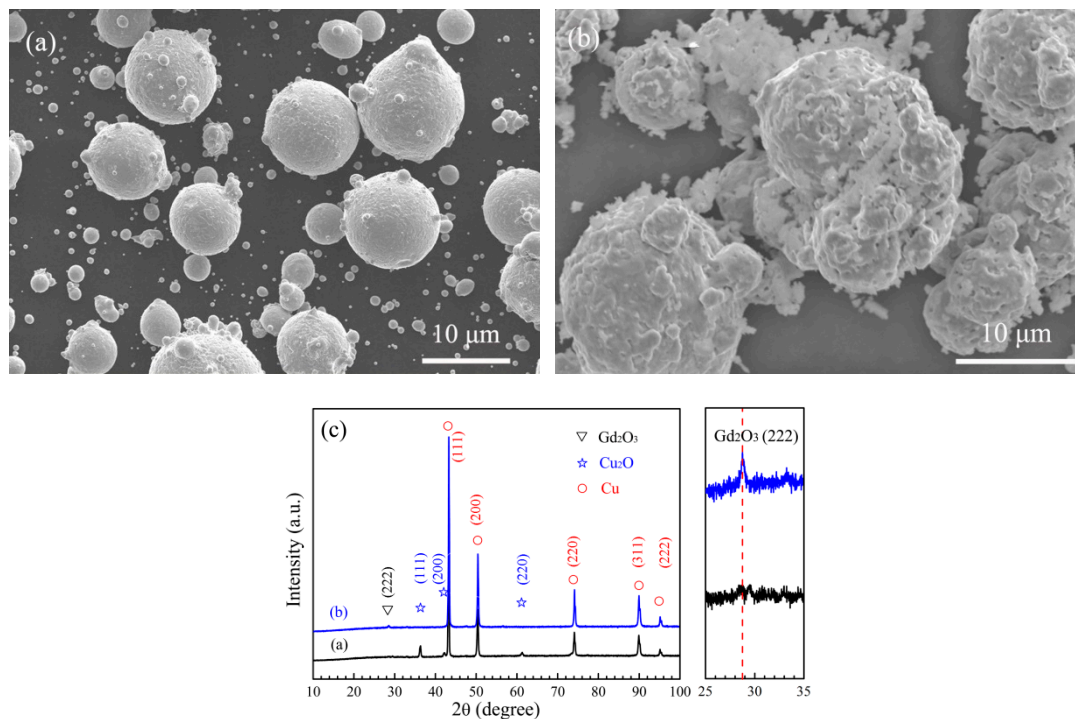


**Figure 4.** The powder analysis of in situ synthesis of Gd<sub>2</sub>O<sub>3</sub>: (a,b) the morphology of Cu-Gd alloy powder mixed with Cu<sub>2</sub>O powder before internal oxidation and after H<sub>2</sub> reduction; (c) the XRD patterns of the mixed powders in Figure 4a,b.

### 3.3. Microstructure

#### 3.3.1. The Distribution of Ti<sub>3</sub>AlC<sub>2</sub> in the Cu Matrix

In order to analyze the effect of electroless Cu plating on the Ti<sub>3</sub>AlC<sub>2</sub> particles and the distribution of the Ti<sub>3</sub>AlC<sub>2</sub> phase in the Cu matrix, the samples of the Ti<sub>3</sub>AlC<sub>2</sub>-Gd<sub>2</sub>O<sub>3</sub>/Cu composite and the Cu@Ti<sub>3</sub>AlC<sub>2</sub>-Gd<sub>2</sub>O<sub>3</sub>/Cu composite were inlaid in one billet for polishing. SEM and EDS images in both composites were collected and their results are shown in Figure 5.

The dark particles with a size of about 2 μm were uniformly distributed in the light-colored area, as shown in Figure 5a,b. From Figure 5a, small cracks and micropores (indicated by red arrows) existed between the dark particles and the matrix in the Ti<sub>3</sub>AlC<sub>2</sub>-Gd<sub>2</sub>O<sub>3</sub>/Cu composite, while the dark particles were closely combined with the matrix without gaps and micropores in the Cu@Ti<sub>3</sub>AlC<sub>2</sub>-Gd<sub>2</sub>O<sub>3</sub>/Cu composite (Figure 5b). Figure 5c shows that the elements in area A in Figure 5b were Ti, Al, C, and Cu, and their atomic percentages were 45.65%, 17.05%, 36.27%, and 1.03%, respectively. The proportion of Cu element was very small, and the ratio of Ti, Al, and C elements was close to 3:1:2, so the dark particle at area A was Ti<sub>3</sub>AlC<sub>2</sub>. All elements in area B in Figure 5b were Cu, indicating that the light-colored area was the Cu matrix.

From Figure 5a, cracks in Ti<sub>3</sub>AlC<sub>2</sub>-Gd<sub>2</sub>O<sub>3</sub>/Cu composites were mainly seen in the interface between the Ti<sub>3</sub>AlC<sub>2</sub> particles and the Cu matrix due to their large misfit in lattice parameters, CTE, and elastic modulus. By electroless plating Cu onto the surface of the Ti<sub>3</sub>AlC<sub>2</sub> particles, the surface contacting state between the Ti<sub>3</sub>AlC<sub>2</sub> particles and Cu matrix was improved and no cracks at the interface were observed in the Cu@Ti<sub>3</sub>AlC<sub>2</sub>-Gd<sub>2</sub>O<sub>3</sub>/Cu composites.

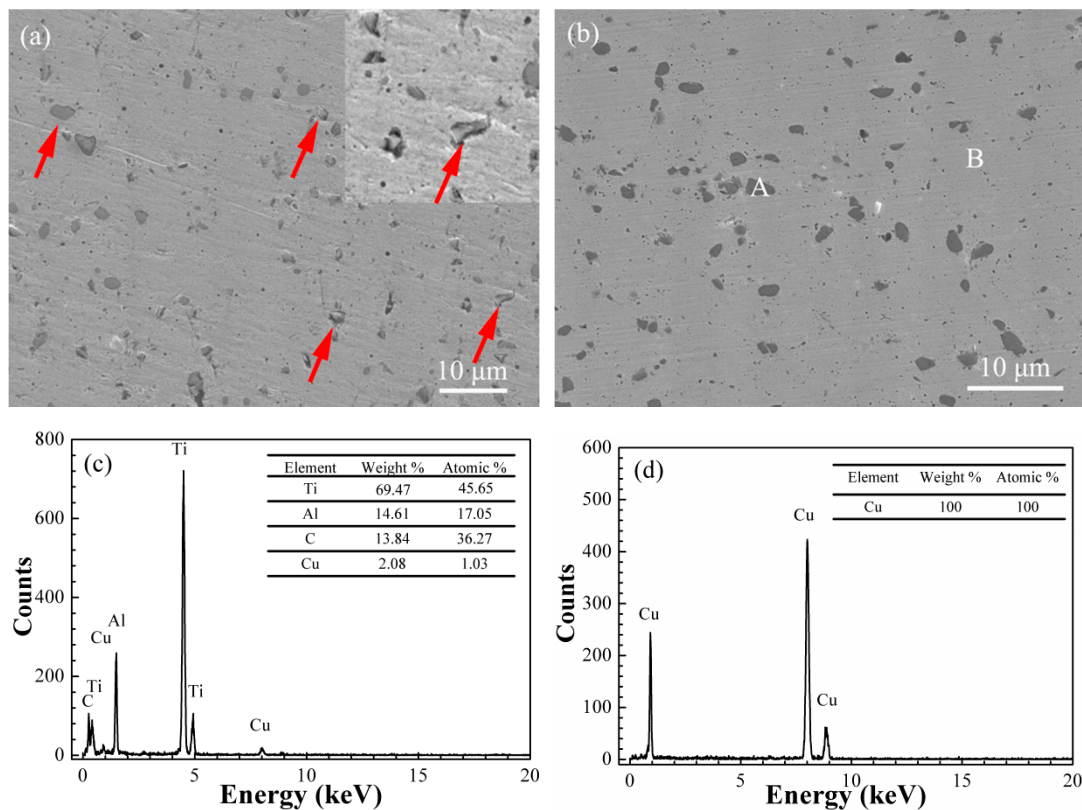


**Figure 5.** The distribution of the  $\text{Ti}_3\text{AlC}_2$  particles in the Cu matrix: (a)  $\text{Ti}_3\text{AlC}_2\text{-Gd}_2\text{O}_3/\text{Cu}$ ; (b)  $\text{Cu@Ti}_3\text{AlC}_2\text{-Gd}_2\text{O}_3/\text{Cu}$ ; (c,d) are the energy spectra of areas A and B in Figure 5b; small cracks and micropores were indicated by red arrows.

### 3.3.2. Microstructure of the $\text{Gd}_2\text{O}_3/\text{Cu}$ Composites

Figure 6 shows the TEM and EDS images of  $\text{Gd}_2\text{O}_3/\text{Cu}$  composite prepared by the internal oxidation method, which was used for further confirming the components of the particles dispersed in the matrix. Figure 6a displays the bright field image, and dark particles (marked as A) and a large bright flat area (marked as B) were selected for EDS analysis. The bright field image showed that the spherical reinforcement phase with a size of about 20  $\mu\text{m}$  was distributed in the matrix. Only Gd, O, and Cu elements existed in the dark area A from the EDS spectrum in Figure 6c, and the atomic percentages of Gd and O elements were 39.53% and 57.30%, their atomic ratio was close to 3:2, illustrating that the spherical reinforcement phase was  $\text{Gd}_2\text{O}_3$ , which was synthesized in the composite during the internal oxidation process. Only Cu existed in area B (Figure 6d), which indicated that the bright area was the Cu matrix.

Further analysis of the high-resolution TEM image of area A in Figure 6a showed that the interplanar spacings of 0.3118 and 0.1802 nm matched with the  $\text{Gd}_2\text{O}_3$  (222) plane (0.3122 nm, PDF 12-0797) and Cu (200) plane (0.1808 nm, PDF 04-0836), respectively (Figure 6b). The  $\text{Gd}_2\text{O}_3$  (222) in Figure 6 was consistent with the XRD result in Figure 4c. The  $\text{Gd}_2\text{O}_3$  particles existed in the Cu matrix without other phases between them due to the in situ nucleation and growth of the  $\text{Gd}_2\text{O}_3$  particles in the Cu matrix, which improved their interface strength and the tensile strength of the  $\text{Gd}_2\text{O}_3/\text{Cu}$  composite.

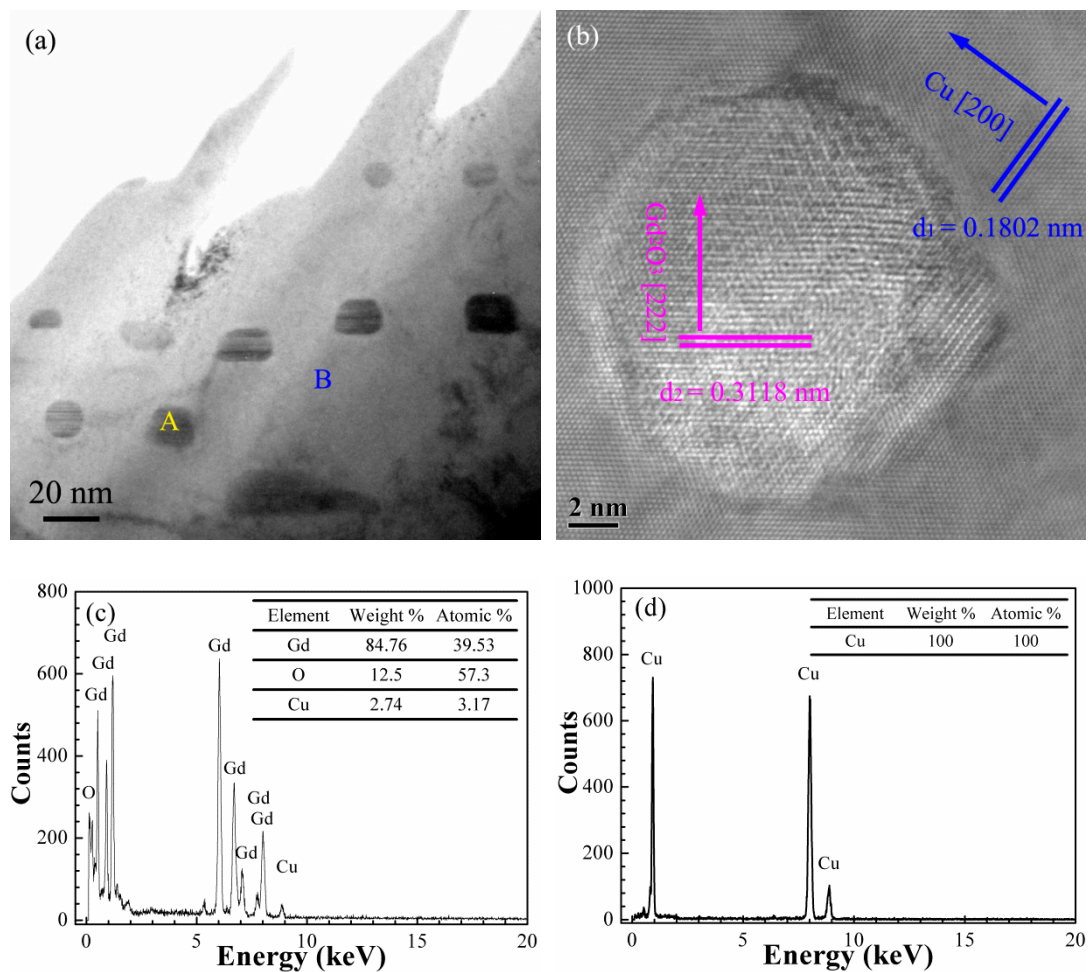


**Figure 6.** The TEM and EDS images of the  $Gd_2O_3/Cu$  composite: (a) bright field image; (b) high resolution image; (c,d) the corresponding EDS spectrum at areas A and B in Figure 6a respectively.

### 3.3.3. Microstructure of the $Ti_3AlC_2-Gd_2O_3/Cu$ Composites

Figure 7a shows the bright field image of the  $Ti_3AlC_2-Gd_2O_3/Cu$  composite, and Figure 7b shows the high-resolution image of the white box in Figure 7a. According to the calibration analysis of the high-resolution image, the interplanar spacings of  $d_1$  and  $d_2$  were 0.2118 and 0.1845 nm, which were highly in accordance with  $Ti_3AlC_2$  (105) plane (0.2159 nm, PDF#52-0875) and Cu (200) plane (0.1808 nm, PDF#04-0836), respectively, because the percentage of the differentials between the test values and the standard values is less than 2%.

There was a micropore between the Cu matrix and the  $Ti_3AlC_2$  particles (the yellow oval in Figure 7a), which might be caused by the high surface energy between the  $Ti_3AlC_2$  particles and the Cu matrix due to their structural characteristics, resulting in the defect during the sintering process. The reinforced phase  $Ti_3AlC_2$  had a clear boundary with the Cu matrix, which was mechanically bound. This indicated that the interfacial bonding between the Cu matrix and the  $Ti_3AlC_2$  particles without Cu plating was weaker, which may weaken the enhancement effect. The result further confirmed the finding in Section 3.3.1.

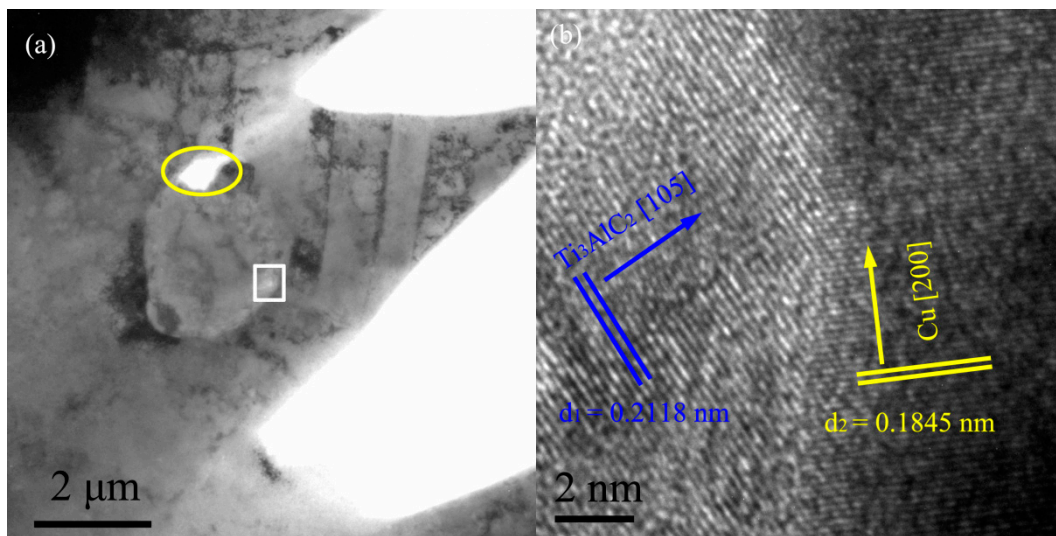


**Figure 7.** The TEM images of the  $\text{Ti}_3\text{AlC}_2\text{-Gd}_2\text{O}_3/\text{Cu}$  composite: (a) bright field image; (b) high resolution image; a micropore was indicated by the yellow circle and the high resolution image was from the white box in Figure 7a.

### 3.3.4. Microstructure of the $\text{Cu@Ti}_3\text{AlC}_2\text{-Gd}_2\text{O}_3/\text{Cu}$ Composites

In order to assess the effect of the electroless Cu plating on the  $\text{Ti}_3\text{AlC}_2$  particles, the TEM images of the  $\text{Cu@Ti}_3\text{AlC}_2\text{-Gd}_2\text{O}_3/\text{Cu}$  composite were collected. Figure 8 presents the TEM and EDS images of  $\text{Cu@Ti}_3\text{AlC}_2\text{-Gd}_2\text{O}_3/\text{Cu}$  composite prepared by electroless Cu plating, internal oxidation, and vacuum hot press sintering.

The fine dark particles were dispersed in the Cu matrix (highlighted by yellow arrows in Figure 8a), which should be the in situ  $\text{Gd}_2\text{O}_3$  inferred by their sizes in Figure 6a. In order to confirm that the dark particles were the in situ  $\text{Gd}_2\text{O}_3$ , the high-resolution TEM image was taken and analyzed as shown in Figure 8c, the interplanar spacings of 0.3151 and 0.2091 nm were in accordance with the  $\text{Gd}_2\text{O}_3$  (222) plane and Cu (111) plane, respectively. The in situ  $\text{Gd}_2\text{O}_3$  particles were in situ nucleated and grew up in the Cu matrix without other phases between them, which improved the tensile strength of the composite. The larger white particles were distributed at the Cu grain boundary in Figure 8a, the EDS (Figure 8b) showed that the main elements in area A were Ti, Al, and C, and only 1.58% of Cu existed, the atomic ratio of Ti, Al, and C elements was close to 3:1:2; the result suggested that the white phase should be  $\text{Ti}_3\text{AlC}_2$ . The high-resolution TEM image at area C was analyzed to further confirm the components. As shown in Figure 8d, the interplanar spacings were 0.2186 and 0.1831 nm and in accordance with the  $\text{Ti}_3\text{AlC}_2$  (105) plane and Cu (200) plane, respectively. Results indicated that the white enhanced phase at area C was  $\text{Ti}_3\text{AlC}_2$ . There were no micropores and cracks between the  $\text{Ti}_3\text{AlC}_2$  particles and the Cu matrix because of the electroless Cu plating on the surface of the  $\text{Ti}_3\text{AlC}_2$  particles.

The in situ  $\text{Gd}_2\text{O}_3$  particles and the  $\text{Ti}_3\text{AlC}_2$  particles in the Cu matrix acted as obstacles to the moving dislocations according to the Orowan strengthening mechanism [28,29], and the dislocation density around the reinforcements in the Cu matrix might be increased due to the thermal expansion coefficient difference between the Cu matrix and reinforcing phase [30,31], leading to an increase in the strength of the  $\text{Cu@Ti}_3\text{AlC}_2\text{-Gd}_2\text{O}_3/\text{Cu}$  composite.

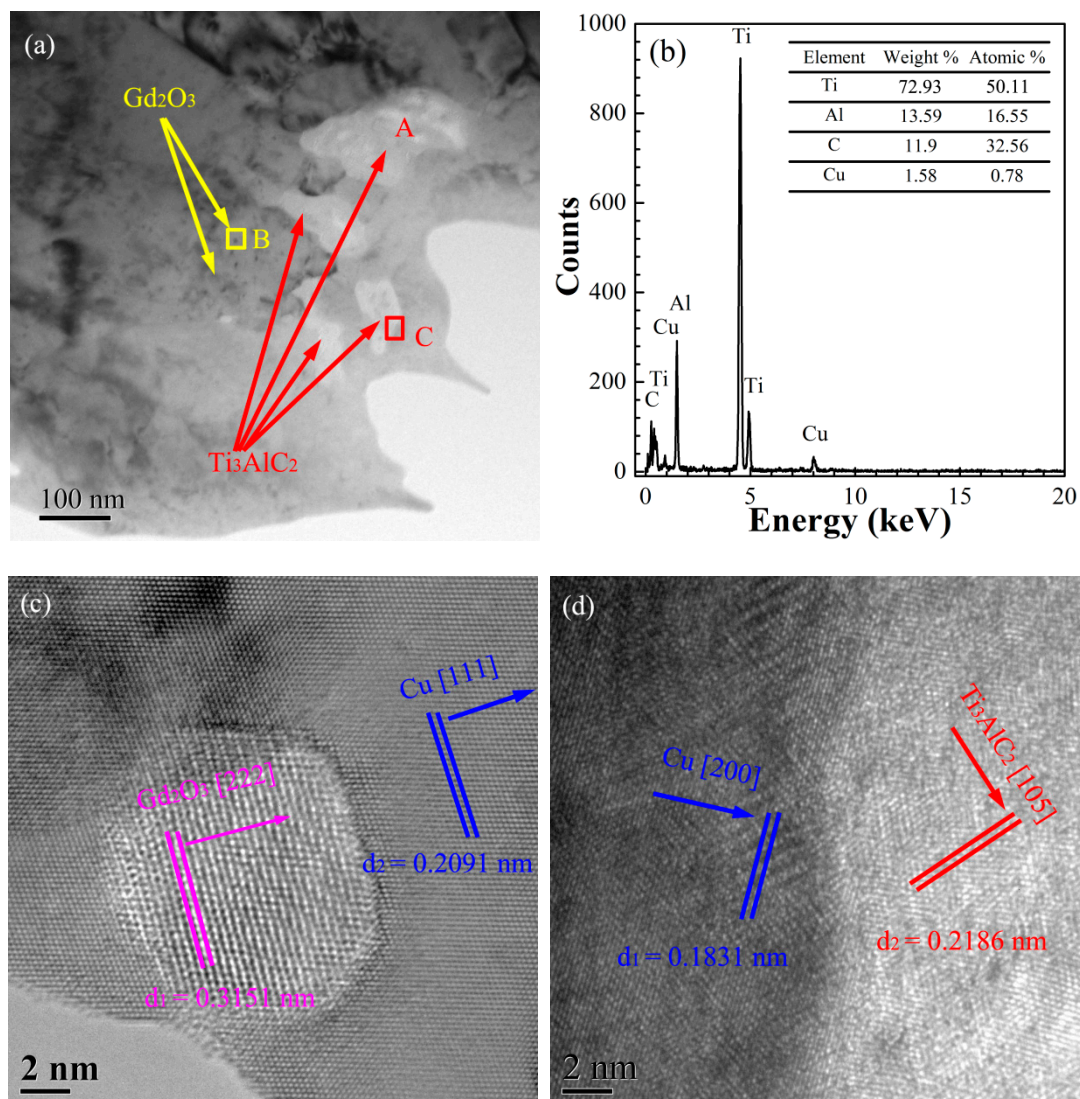


**Figure 8.** The TEM and EDS images of  $\text{Cu@Ti}_3\text{AlC}_2\text{-Gd}_2\text{O}_3/\text{Cu}$  composite: (a) the bright field image; (b) the energy spectra of area A in Figure 8a; (c,d) are the high-resolution images of areas B and C in Figure 8a, respectively.

### 3.4. Tensile Strength and Electrical Conductivity

Figure 9 shows the stress–strain curve (a), tensile strength and electrical conductivity (b) of three different composites:  $\text{Gd}_2\text{O}_3/\text{Cu}$  composite, the  $\text{Ti}_3\text{AlC}_2\text{-Gd}_2\text{O}_3/\text{Cu}$  composite, and the  $\text{Cu@Ti}_3\text{AlC}_2\text{-Gd}_2\text{O}_3/\text{Cu}$  composite.

As could be seen from Figure 9a, a large plastic deformation occurred before fracture during the tensile test, the tensile strength was improved by ex situ  $\text{Ti}_3\text{AlC}_2$  particles from 325.4 ( $\text{Gd}_2\text{O}_3/\text{Cu}$  composite) to 351.4 MPa ( $\text{Ti}_3\text{AlC}_2\text{-Gd}_2\text{O}_3/\text{Cu}$  composite), the modulus of the  $\text{Ti}_3\text{AlC}_2\text{-Gd}_2\text{O}_3/\text{Cu}$  composite was also increased at the same time, but the elongation decreased from  $26.1 \pm 0.2\%$  to  $15.2 \pm 0.3\%$ . After electroless Cu plating on the surface of the  $\text{Ti}_3\text{AlC}_2$  particles, the tensile strength of the  $\text{Cu@Ti}_3\text{AlC}_2\text{-Gd}_2\text{O}_3/\text{Cu}$  composite was further increased to 378.9 MPa and elongation at break reached  $17.6 \pm 0.2\%$ . The tensile strength and elongations of the  $\text{Cu@Ti}_3\text{AlC}_2\text{-Gd}_2\text{O}_3/\text{Cu}$  composite were improved by 27.5 MPa and 2.4%, respectively, comparing with the  $\text{Ti}_3\text{AlC}_2\text{-Gd}_2\text{O}_3/\text{Cu}$  composite. The electrical conductivity decreased slightly from 95.0% IACS of the  $\text{Gd}_2\text{O}_3/\text{Cu}$  composite to 92.9% IACS of  $\text{Ti}_3\text{AlC}_2\text{-Gd}_2\text{O}_3/\text{Cu}$  composite by directly adding  $\text{Ti}_3\text{AlC}_2$  particles, but it still remained above 90.0% IACS. Comparing with the  $\text{Ti}_3\text{AlC}_2\text{-Gd}_2\text{O}_3/\text{Cu}$  composite without electroless Cu plating on the surface of the  $\text{Ti}_3\text{AlC}_2$ , the electrical conductivity of the  $\text{Cu@Ti}_3\text{AlC}_2\text{-Gd}_2\text{O}_3/\text{Cu}$  composite was improved by 2.4%, respectively, comparing with the  $\text{Ti}_3\text{AlC}_2\text{-Gd}_2\text{O}_3/\text{Cu}$  composite.

Gd<sub>2</sub>O<sub>3</sub>/Cu composite with Cu plating was slightly increased to 93.6%IACS. The electrical conductivity and elongation of the Cu@Ti<sub>3</sub>AlC<sub>2</sub>-Gd<sub>2</sub>O<sub>3</sub>/Cu composites prepared by the combination of in situ synthesized and ex situ added methods were 93.6%IACS and 17.6% (this paper), which were much higher than that of the TiB<sub>2</sub>/Cu composite in [9]. However, the tensile strength of the Cu@Ti<sub>3</sub>AlC<sub>2</sub>-Gd<sub>2</sub>O<sub>3</sub>/Cu composite was lower than that of the TiB<sub>2</sub>/Cu composite because 1 wt% Fe was added into the TiB<sub>2</sub>/Cu composite.

Comparing with the Gd<sub>2</sub>O<sub>3</sub>/Cu composite, the tensile strength increase in the Ti<sub>3</sub>AlC<sub>2</sub>-Gd<sub>2</sub>O<sub>3</sub>/Cu composite was due to the pinning of the dislocation movement caused by the in situ Gd<sub>2</sub>O<sub>3</sub> particles in the Cu grains and the Ti<sub>3</sub>AlC<sub>2</sub> particles at the boundary of the Cu grains according to the grain boundary strengthening, Orowan strengthening, thermal mismatch strengthening, and load transfer strengthening mechanisms [29,32–34]. The decrease in electrical conductivity in the Ti<sub>3</sub>AlC<sub>2</sub>-Gd<sub>2</sub>O<sub>3</sub>/Cu composite was due to the electron concentration decrease and the increases in free electron scattering caused by the Ti<sub>3</sub>AlC<sub>2</sub> particles at the Cu grain boundary [35]. Comparing with the Ti<sub>3</sub>AlC<sub>2</sub>-Gd<sub>2</sub>O<sub>3</sub>/Cu composite, the tensile strength and electrical conductivity of the Cu@Ti<sub>3</sub>AlC<sub>2</sub>-Gd<sub>2</sub>O<sub>3</sub>/Cu composite were simultaneously increased because the surfactivity between the Cu matrix and the Ti<sub>3</sub>AlC<sub>2</sub> particles was reduced after electroless Cu plating on their surface, which led to the better surface contacting state and less electron scattering after sintering.

For the Ti<sub>3</sub>AlC<sub>2</sub>-Gd<sub>2</sub>O<sub>3</sub>/Cu composite, the load would be transferred from the Cu matrix to the Ti<sub>3</sub>AlC<sub>2</sub> particles during the tensile test, which hindered the plastic deformation of the Cu matrix and reduced its elongation. With the addition of Cu@Ti<sub>3</sub>AlC<sub>2</sub> particles into the Gd<sub>2</sub>O<sub>3</sub>/Cu composite, the interfacial bonding between the Cu@Ti<sub>3</sub>AlC<sub>2</sub> particles and Cu matrix was improved due to the Cu plating on the surface of the Ti<sub>3</sub>AlC<sub>2</sub> particles. The opportunity of crack initiation between the Cu@Ti<sub>3</sub>AlC<sub>2</sub> particles and Cu matrix was low under the same load condition, resulting in the continuous plastic deformation of the Cu matrix, so increased tensile strength and elongation of Cu@Ti<sub>3</sub>AlC<sub>2</sub>-Gd<sub>2</sub>O<sub>3</sub>/Cu composite were seen.

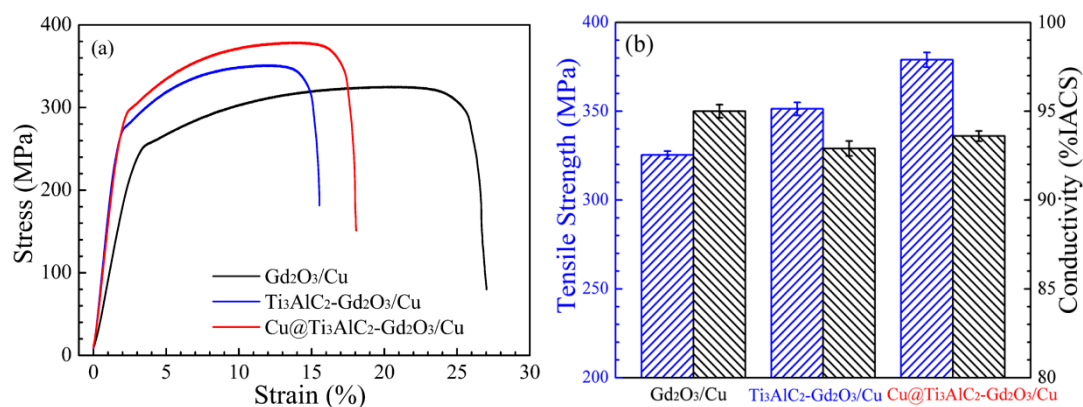


**Figure 9.** The stress–strain curve, tensile strength, and electrical conductivity of the composites: (a) the stress–strain curve and (b) the tensile strength and electrical conductivity.

### 3.5. Fracture Morphology

A large number of dimples with uniform sizes distributed on the fracture surface of the Gd<sub>2</sub>O<sub>3</sub>/Cu composites are shown in Figure 10a, and these typical ductile fractures indicated that the Gd<sub>2</sub>O<sub>3</sub>/Cu composite was plastically deformed before fracture. The enlarged image in Figure 10b showed in situ Gd<sub>2</sub>O<sub>3</sub> particles existing at the bottom of the dimples, which proved the movement of the dislocation would be impeded by the in situ Gd<sub>2</sub>O<sub>3</sub> particles during the tensile test and helped to improve the tensile strength of the Gd<sub>2</sub>O<sub>3</sub>/Cu composite [26,27]. The size of the in situ Gd<sub>2</sub>O<sub>3</sub> particles was about 20 nm, and the value was consistent with the results in Figure 6a,b and Figure 8c.

There were relatively obvious gaps between the Cu matrix and the Ti<sub>3</sub>AlC<sub>2</sub> particles in the fracture morphology of the Ti<sub>3</sub>AlC<sub>2</sub>-Gd<sub>2</sub>O<sub>3</sub>/Cu composite (Figure 10c,d), and Ti<sub>3</sub>AlC<sub>2</sub>

particles with a size of about 2  $\mu\text{m}$  existed at the bottom of the dimples. After electroless Cu plating on the surface of the  $\text{Ti}_3\text{AlC}_2$  particles, no gaps existed in the  $\text{Cu@Ti}_3\text{AlC}_2\text{-Gd}_2\text{O}_3/\text{Cu}$  composite, as shown in Figure 10e,f, and it could be seen that dimples with uniform size were distributed in the fracture morphology of the  $\text{Cu@Ti}_3\text{AlC}_2\text{-Gd}_2\text{O}_3/\text{Cu}$  composite.

The reason for the gaps formed in the  $\text{Ti}_3\text{AlC}_2\text{-Gd}_2\text{O}_3/\text{Cu}$  composite might be the weak interface bonding due to their large misfit in lattice parameters, CTE, and elastic modulus between the  $\text{Ti}_3\text{AlC}_2$  particles and the Cu matrix. During the tensile testing process, the load would be transferred from the Cu matrix to  $\text{Ti}_3\text{AlC}_2$  particles via the interface; with the increase in the load, the  $\text{Ti}_3\text{AlC}_2$  particles could hinder the dislocation movement so that the tensile strength of the  $\text{Ti}_3\text{AlC}_2\text{-Gd}_2\text{O}_3/\text{Cu}$  composite was improved. As the load increased further to the level that exceeded the interface bonding strength, the cracks initiated from the interface between  $\text{Ti}_3\text{AlC}_2$  particles and Cu matrix and interface debonding happened, so the gaps between  $\text{Ti}_3\text{AlC}_2$  particles and Cu matrix were observed. With the electroless Cu plating onto the surface of the  $\text{Ti}_3\text{AlC}_2$  particles, the surfactivity between the  $\text{Cu@Ti}_3\text{AlC}_2$  particles and the Cu matrix was reduced, and a better surface contacting state was achieved after the sintering process, so that no interface debonding was formed between the  $\text{Cu@Ti}_3\text{AlC}_2$  particles and the Cu matrix during the tensile process. Higher tensile strength and elongation was achieved in the  $\text{Cu@Ti}_3\text{AlC}_2\text{-Gd}_2\text{O}_3/\text{Cu}$  composite.

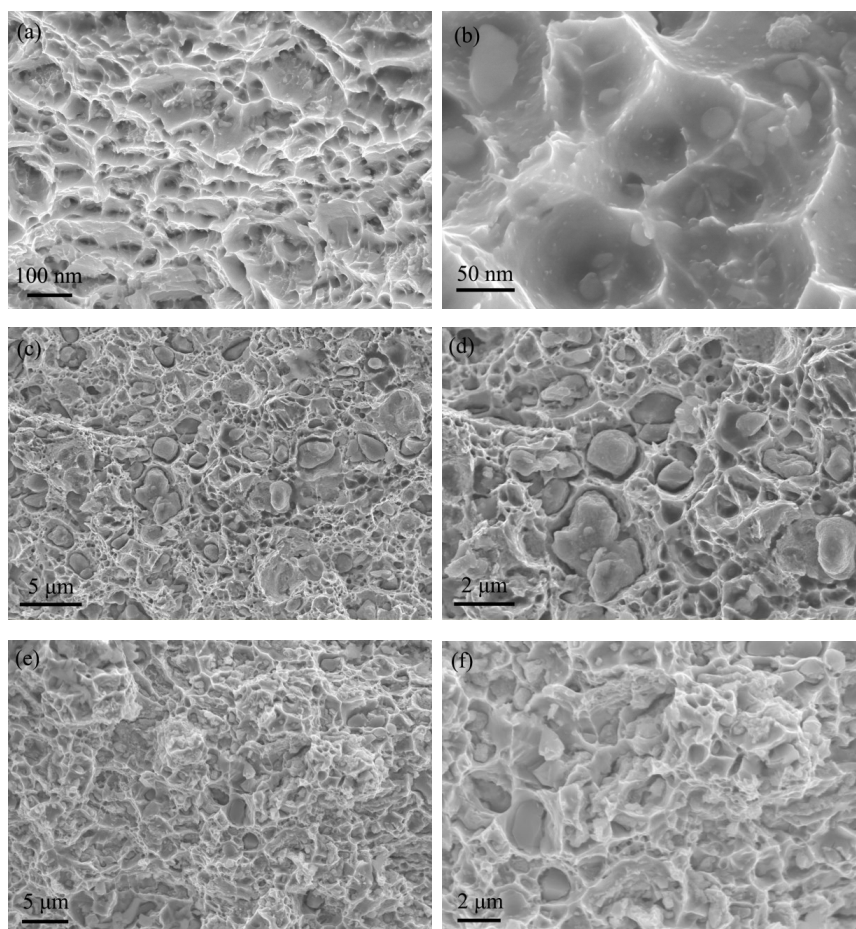


**Figure 10.** The fracture morphology of the composites: (a,b) the  $\text{Gd}_2\text{O}_3/\text{Cu}$  composite; (c,d) the  $\text{Ti}_3\text{AlC}_2\text{-Gd}_2\text{O}_3/\text{Cu}$  composite; (e,f) the  $\text{Cu@Ti}_3\text{AlC}_2\text{-Gd}_2\text{O}_3/\text{Cu}$  composite.

#### 4. Conclusions

According to the preparation and performance analysis of the Cu@Ti<sub>3</sub>AlC<sub>2</sub>-Gd<sub>2</sub>O<sub>3</sub>/Cu composites, Ti<sub>3</sub>AlC<sub>2</sub>-Gd<sub>2</sub>O<sub>3</sub>/Cu composites, and Gd<sub>2</sub>O<sub>3</sub>/Cu composites, the innovation points of the combination method and the composites with high tensile strength and electrical conductivity were achieved, and the major findings were as follows:

The Cu@Ti<sub>3</sub>AlC<sub>2</sub>-Gd<sub>2</sub>O<sub>3</sub>/Cu composites with high tensile strength and electrical conductivity were prepared using the combination method of in situ synthesized and ex situ added reinforcement phase.

The Gd<sub>2</sub>O<sub>3</sub> particles were in situ synthesized during the internal oxidation, and the Gd<sub>2</sub>O<sub>3</sub> particles with a size of about 20 nm were dispersed in the Cu grains. The Ti<sub>3</sub>AlC<sub>2</sub> particles were successfully wrapped by a Cu plating without gaps and micropores, which existed at the Cu grain boundary.

The interfacial bonding between the Ti<sub>3</sub>AlC<sub>2</sub> particles and Cu matrix was effectively improved by the Cu plating onto the surface of Ti<sub>3</sub>AlC<sub>2</sub> particles, and the tensile strength, reached 378.9 MPa, meanwhile, electrical conductivity and elongation of the Cu@Ti<sub>3</sub>AlC<sub>2</sub>-Gd<sub>2</sub>O<sub>3</sub>/Cu composites remained at 93.6 IACS% and 17.6%.

Only the reinforcement by in situ rare earth oxides and ex situ MAX phases were characterized in this paper, and reinforcements using other particles in Cu matrix composites will be studied in the future.

**Author Contributions:** Conceptualization, H.C., Z.Z.; methodology, H.C., Z.Z., X.L.; validation, H.C., Z.Z.; formal analysis, H.C., X.L.; investigation, H.C., Z.Z.; data curation, H.C., Z.Z.; writing—original draft preparation, H.C., Z.Z.; writing—review and editing, H.C., Z.Z., X.L.; supervision, H.C., Z.Z., X.L. All authors have read and agreed to the published version of the manuscript.

**Funding:** This work was supported by the Natural Science Foundation of Hebei Province (grant number E2017203298).

**Institutional Review Board Statement:** Not applicable.

**Informed Consent Statement:** Not applicable.

**Data Availability Statement:** Data is contained within the article.

**Conflicts of Interest:** The authors declare no conflict of interest.

#### References

1. Peng, J.; Chen, B.; Wang, Z.; Guo, J.; Wu, B.; Hao, S.; Zhang, Q.; Gu, L.; Zhou, Q.; Liu, Z.; et al. Surface coordination layer passivates oxidation of copper. *Nature* **2020**, *586*, 390–394. [[CrossRef](#)] [[PubMed](#)]
2. Zhang, S.; Kang, H.; Wang, Z.; Guo, E.; Chen, Z.; Wang, T. Microstructure and properties of dual-scale particulate reinforced copper matrix composites with superior comprehensive properties. *J. Alloy. Compd.* **2021**, *860*, 157888. [[CrossRef](#)]
3. Ma, B.; Hishinuma, Y.; Noto, H.; Shimada, Y.; Muroga, T. Development of Y<sub>2</sub>O<sub>3</sub> dispersion strengthened Cu alloy using Cu<sub>6</sub>Y and Cu<sub>2</sub>O addition through the MA-HIP process. *Fusion Eng. Des.* **2020**, *161*, 112045. [[CrossRef](#)]
4. Huang, B.; Ma, B.; Hishinuma, Y.; Noto, H.; Muroga, T. Investigations on the formation of multi-modal size distribution of mechanochemically processed Cu-Y-CuO powders. *Fusion Eng. Des.* **2020**, *158*, 111852. [[CrossRef](#)]
5. Cao, H.; Zhan, Z.; Lv, X. Microstructure Evolution and Properties of an In-Situ Nano-Gd<sub>2</sub>O<sub>3</sub>/Cu Composite by Powder Metallurgy. *Materials* **2021**, *14*, 5021. [[CrossRef](#)]
6. Chandrasekhar, S.B.; Sudhakara Sarma, S.; Ramakrishna, M.; Suresh Babu, P.; Rao, T.N.; Kashyap, B.P. Microstructure and properties of hot extruded Cu-1wt% Al<sub>2</sub>O<sub>3</sub> nano-composites synthesized by various techniques. *Mater. Sci. Eng. A* **2014**, *591*, 46–53. [[CrossRef](#)]
7. Güler, O.; Varol, T.; Alver, Ü.; Canakci, A. Effect of Al<sub>2</sub>O<sub>3</sub> content and milling time on the properties of silver coated Cu matrix composites fabricated by electroless plating and hot pressing. *Mater. Today Commun.* **2020**, *24*, 101153. [[CrossRef](#)]
8. Wang, X.; Li, J.; Zhang, Y.; Wang, Y. Improvement of interfacial bonding and mechanical properties of Cu-Al<sub>2</sub>O<sub>3</sub> composite by Cr-nanoparticle-induced interfacial modification. *J. Alloy. Compd.* **2017**, *695*, 2124–2130. [[CrossRef](#)]
9. Pan, S.; Zheng, T.; Yao, G.; Chi, Y.; Rosa, I.D.; Li, X. High-strength and high-conductivity in situ Cu-TiB<sub>2</sub> nanocomposites. *Mater. Sci. Eng. A* **2022**, *831*, 141952. [[CrossRef](#)]
10. Hwang, J.; Yoon, T.; Jin, S.H.; Lee, J.; Kim, T.; Hong, S.H.; Jeon, S. Enhanced Mechanical Properties of Graphene/Copper Nanocomposites Using a Molecular-Level Mixing Process. *Adv. Mater.* **2013**, *25*, 6724–6729. [[CrossRef](#)]

11. Zhuo, H.; Tang, J.; Ye, N. A novel approach for strengthening Cu-Y<sub>2</sub>O<sub>3</sub> composites by in situ reaction at liquidus temperature. *Mater. Sci. Eng. A* **2013**, *584*, 1–6. [[CrossRef](#)]
12. Kudashov, D.V.; Baum, H.; Martin, U.; Heilmaier, M.; Oettel, H. Microstructure and room temperature hardening of ultra-fine-grained oxide-dispersion strengthened copper prepared by cryomilling. *Mater. Sci. Eng. A* **2004**, *387–389*, 768–771. [[CrossRef](#)]
13. Shabadi, R.; Avettand-Fènoël, M.N.; Simar, A.; Taillard, R.; Jain, P.K.; Johnson, R. Thermal conductivity in yttria dispersed copper. *Mater. Des.* **2015**, *65*, 869–877. [[CrossRef](#)]
14. Mo, F.; Feng, Y.; Chen, Y.; Wang, Y.; Qian, G.; Dou, Y.; Zhang, X. Effect of La<sub>2</sub>O<sub>3</sub> on electrical friction and wear properties of Cu-graphite composites. *J. Rare Earths.* **2015**, *33*, 327–333. [[CrossRef](#)]
15. Groza, J.R.; Gibeling, J.C. Principles of particle selection for dispersion-strengthened copper. *Mater. Sci. Eng. A* **1993**, *171*, 115–125. [[CrossRef](#)]
16. Zheng, R.; Zhan, Z.; Wang, W. Wear behavior of Cu-La<sub>2</sub>O<sub>3</sub> composite with or without electrical current. *Wear* **2010**, *268*, 72–76. [[CrossRef](#)]
17. Aghamiri, S.M.S.; Oono, N.; Ukai, S.; Kasada, R.; Noto, H.; Hishinuma, Y.; Muroga, T. Microstructure development and high tensile properties of He/H<sub>2</sub> milled oxide dispersion strengthened copper. *J. Alloy. Compd.* **2019**, *783*, 674–679. [[CrossRef](#)]
18. Huang, F.; Wang, H.; Yang, B.; Liao, T.; Wang, Z. Uniformly dispersed Y<sub>2</sub>O<sub>3</sub> nanoparticles in nanocrystalline copper matrix via multi-step ball milling and reduction process. *Mater. Lett.* **2019**, *242*, 119–122. [[CrossRef](#)]
19. Hu, W.; Huang, Z.; Wang, Y.; Li, X.; Zhai, H.; Zhou, Y.; Chen, L. Layered ternary MAX phases and their MX particulate derivative reinforced metal matrix composite: A review. *J. Alloy. Compd.* **2021**, *586*, 517313. [[CrossRef](#)]
20. Sobolev, K.; Gorshenkov, M.; Manfrinetti, P.; Peddis, D.; Pazniak, A.; Rodionova, V. Synthesis of phase-pure highly-doped MAX-phase (Cr<sub>1-x</sub>Mn<sub>x</sub>)<sub>2</sub>AlC. *Ceram. Inf.* **2021**, *47*, 21069–21076. [[CrossRef](#)]
21. Wang, W.; Zhai, H.; Chen, L.; Zhou, Y.; Huang, Z.; Bei, G.; Greil, P. Sintering and properties of mechanical alloyed Ti<sub>3</sub>AlC<sub>2</sub>-Cu composites. *Mater. Sci. Eng. A* **2017**, *685*, 154–158. [[CrossRef](#)]
22. Griseri, M.; Tunca, B.; Lapauw, T.; Huang, S.; Popescu, L.; Barsoum, M.W.; Lambrinou, K.; Vleugels, J. Synthesis, properties and thermal decomposition of the Ta<sub>4</sub>AlC<sub>3</sub> MAX phase. *J. Eur. Ceram. Soc.* **2019**, *39*, 2973–2981. [[CrossRef](#)]
23. Badie1, S.; Dash, A.; Sohn, Y.J.; Vaßen, R.; Guillon, O. Gonzalez-Julian, J. Synthesis, sintering, and effect of surface roughness on oxidation of submicron Ti<sub>2</sub>AlC ceramics. *J. Am. Ceram. Soc.* **2021**, *104*, 1669–1688. [[CrossRef](#)]
24. Was'kowska, A.; Gerward, L.; Olsen, J.S.; Babu, K.R.; Vaitheeswaran, G.; Kanchana, V.; Svane, A.; Filipov, V.B.; Levchenko, G.; Lyaschenko, A. Thermoelastic properties of ScB<sub>2</sub>, TiB<sub>2</sub>, YB<sub>4</sub> and HoB<sub>4</sub>: Experimental and theoretical studies. *Acta Mater.* **2011**, *59*, 4886–4894. [[CrossRef](#)]
25. Guo, M.; Shen, K.; Wang, M. Relationship between microstructure, properties and reaction conditions for Cu-TiB<sub>2</sub> alloys prepared by in situ reaction. *Acta Mater.* **2009**, *57*, 4568–4579. [[CrossRef](#)]
26. Magnuson, M.; Wilhelmsson, O.; Palmquist, J.-P.; Jansson, U.; Mattesini, M.; Li, S.; Ahuja, R.; Eriksson, O. Electronic structure and chemical bonding in Ti<sub>2</sub>AlC investigated by soft x-ray emission spectroscopy. *Phys. Rev. B* **2006**, *74*, 195180. [[CrossRef](#)]
27. Gonzalez-Julian, J. Processing of MAX phases: From synthesis to applications. *J. Am. Ceram. Soc.* **2021**, *104*, 659–690. [[CrossRef](#)]
28. Hao, Z.; Hao, Z.; Xie, G.; Liu, X.; Tan, Q.; Wang, R. The precipitation behaviours and strengthening mechanism of a Cu-0.4 wt% Sc alloy. *J. Mater. Sci. Technol.* **2022**, *98*, 1–13. [[CrossRef](#)]
29. Ma, K.; Wen, H.; Hu, T.; Topping, T.D.; Isheim, D.; Seidman, D.N.; Lavernia, E.J.; Schoenung, J.M. Mechanical behavior and strengthening mechanisms in ultrafine grain precipitation-strengthened aluminum alloy. *Acta Mater.* **2014**, *62*, 141–155. [[CrossRef](#)]
30. Arsenault, R.J.; Shi, N. Dislocation generation due to differences between the coefficients of thermal expansion. *Mater. Sci. Eng.* **1986**, *81*, 175–187. [[CrossRef](#)]
31. Dunand, D.C.; Mortensen, A. Reinforced silver chloride as a model material for the study of dislocations in metal matrix composites. *Mater. Sci. Eng. A* **1991**, *144*, 179–188. [[CrossRef](#)]
32. Deng, K.; Shi, J.; Wang, C.; Wang, X.; Wu, Y.; Nie, K.; Wu, K. Microstructure and strengthening mechanism of bimodal size particle reinforced magnesium matrix composite. *Compos. Part A Appl. Sci. Manuf.* **2012**, *43*, 1280–1284. [[CrossRef](#)]
33. Xiong, B.; Yu, H.; Xu, Z.; Yan, Q.; Cai, C. Fabrication of SiC particulate reinforced AZ91D composite by vacuum-assisted pressure infiltration technology. *J. Alloy. Compd.* **2011**, *509*, L279–L283. [[CrossRef](#)]
34. Yan, S.; Dai, S.; Zhang, X.; Yang, C.; Hong, Q.; Chen, J.; Lin, Z. Investigating aluminum alloy reinforced by graphene nanoflakes. *Mater. Sci. Eng. A* **2014**, *612*, 440–444. [[CrossRef](#)]
35. Pan, S.; Yuan, J.; Zhang, P.; Sokoluk, M.; Yao, G.; Li, X. Effect of electron concentration on electrical conductivity in in situ Al-TiB<sub>2</sub> nanocomposites. *Appl. Phys. Lett.* **2020**, *116*, 014102. [[CrossRef](#)]